arXiv:1402.4137v3 [astro-ph.GA] 19 Jun 2015

Progenitors of Supernovae Type Ia and Chemical Enrichment in Hydrodynamical Simulations -I. The Single Degenerate Scenario

Noelia Jiménez[1,2,5,8], Patricia B. Tissera[2,3,4], and Francesca Matteucci[5,6,7]
nj22@st-andrews.ac.uk

ABSTRACT

The nature of the Type Ia supernovae (SNIa) progenitors remains still uncertain. This is a major issue for galaxy evolution models since both chemical and energetic feedback play a major role in the gas dynamics, star formation and therefore in the overall stellar evolution. The progenitor models for the SNIa available in the literature propose different distributions for regulating the explosion times of these events. These functions are known as the Delay Time Distributions (DTDs). This work is the first one in a series of papers aiming at studying five different DTDs for SNIa. Here, we implement and analyse the Single Degenerate scenario (SD) in galaxies dominated by a rapid quenching of the star formation, displaying the majority of the stars concentrated in the bulge component. We find a good fit to both the present observed SNIa rates in spheroidal dominated galaxies, and to the [O/Fe] ratios shown by the bulge of the Milky Way. Additionally, the SD scenario is found to reproduce a correlation between the specific SNIa rate and the specific star formation rate, which closely resembles the observational trend, at variance with previous works. Our results suggest that SNIa observations in galaxies with very low and very high specific star formation rates can help to impose more stringent constraints on the DTDs and therefore on SNIa progenitors.

Subject headings: galaxies: general– galaxies: abundances – galaxies: evolution – Galaxy:bulge–methods: numerical–hydrodynamics

1. Introduction

Galaxy formation represents a multi-scale highly non-linear process. The modeling of the observed galaxy populations with a self-consistent model – from the initial conditions left behind the Big Bang–, requires knowledge of the co-evolution of all the components of the Universe. According to the Λ-Cold Dark Matter (ΛCDM) paradigm, baryons condensate onto the dark matter haloes, which constitute the sites of galaxy formation. The theories of galaxy formation aim at understanding at the same time the large scale growth of the structure and small-scales processes such as the star formation from molecular clouds, for example. This is a challenging task which can be tackled by using semi-analytical or fully cosmological models. Both, resort to recipes or sub-grid modeling to include complex physical processes which cannot be numerically resolved. Hence, is of utmost importance to confront the model results with observations to learn about galaxy formation and to test the validity of the adopted hypotheses.

[1]School of Physics & Astronomy, University of St Andrews, North Haugh, St Andrews, KY16 9SS, Scotland, UK

[2]Instituto de Astronomía y Física del Espacio (IAFE, CONICET-UBA), CC. 67 Suc. 28, C1428ZAA, Ciudad de Buenos Aires, Argentina

[3]Departamento de Ciencias Fisicas, Universidad Andres Bello, Av. Republica 220, Santiago,Chile

[4]Millenium Institute of Astrophysics, Santiago, Chile

[5]Dipartimento di Fisica, Universita' di Trieste, Via G. B. Tiepolo, 11, 34100, Trieste

[6]INAF,Trieste, Via G. B. Tiepolo, 11, 34100, Trieste

[7]I.N.F.N., Via Valerio 2, 34100, Trieste

[8]Institut d' Estudis Espacials de Catalunya (IEEC), Institut de Ciencies de L'Espai (ICE), Spain

Galaxy chemical evolution models provides us with a powerful tool to understand the way in which galaxies formed and evolved (Tinsley 1979; Matteucci & Greggio 1986; Matteucci 1994). Since the information given by chemical abundances is the result of the nucleosynthesis production of the stellar populations and large scale physics involved in the galaxy formation, chemical patterns can provide stringent constraints for galaxy formation models.

The treatment of chemical evolution with the inclusion of different models for Type Ia supernovae (SNeIa) opened the route to study galaxy formation by probing links between chemical patterns and relevant physical processes. These efforts are usually attempted with a variety of numerical techniques, such as multi-zone chemical evolution models (e.g. Matteucci & Greggio 1986; Bravo et al. 1993; Chiappini et al. 2001; Pipino & Matteucci 2004), semi-analytic models of galaxy formation (e.g. Calura & Menci 2009; Arrigoni et al. 2010; Jiménez et al. 2011; Yates et al. 2013; De Lucia et al. 2014; Gargiulo et al. 2015), and cosmological hydrodynamical simulations (e.g. Raiteri et al. 1996; Carraro et al. 1998; Mosconi et al. 2001; Tornatore et al. 2004; Nakasato & Nomoto 2003; Kobayashi 2004; Scannapieco et al. 2005; Nagashima et al. 2005; Wiersma et al. 2009; Aumer et al. 2013; Few et al. 2014, to name a few). Nowadays, sophisticated computational tools and detailed observations of local and high redshift galaxies enable us to improve galaxy formation models and develop more realistic schemes for the baryonic astrophysics.

One of the major astrophysical problems is the uncertain identity of the SNIa progenitors. This is a matter of concern not only in galaxy formation theory but also in modern cosmology. The remarkable similarity shown by the light curves of the SNIa have made them excellent cosmological distance indicators. Hence, they are used to investigate the properties of dark energy, and to test parameters of the cosmological model and the acceleration epoch of the Universe (Perlmutter et al. 1999). However, given the still unknown nature of the progenitor systems of SNIa, systematic errors in the deduced distances based on calibrations of nearby SNeIa, could have an impact in the cosmological parameter estimation (Pan et al. 2012; Rest et al. 2013).

It is well known that core-collapse supernovae (SNeII) are produced by massive short-lived stars (M$>$ 8 M$_{\odot}$). The nucleosynthesis production of these events feeds the interstellar medium (ISM) with energy and, mainly, with the so-called α-elements – O, Ne, Mg, Si, S and Ca –. On the other hand, the SNeIa are the main contributor of the Fe in the Universe (Greggio & Renzini 1983; Matteucci & Greggio 1986; Cappellaro et al. 1997). This element is usually considered to be a tracer of the metallicity in stars. Furthermore, the production and distribution of the chemical elements in the ISM affects the cooling rates of the gas (Sutherland & Dopita 1993), the star formation processes, the subsequent stellar evolution (Pietrinferni et al. 2006), and the production of high-redshift dust (Maiolino et al. 2004; Bianchi & Schneider 2007). Main properties such as the luminosity function and the mass distribution of galaxies might consequently be affected (White & Frenk 1991; Scannapieco et al. 2005). By studying the enhancement of the α-elements relative to Fe, we expect to learn about the Initial Mass Function (IMF) of the stellar populations and, very importantly, about the time-scales in which SNeIa become relevant. The time-delay between core-collapse SNe and SNeIa injection of chemical elements in the ISM, creates important patterns which can be used as clocks to tag particular events in the formation histories of galaxies. Given a starburst, SNIa events occur following a distribution of explosion times which is known as the Delay Time Distribution (DTD). Different scenarios for SNIa progenitors produce different DTDs which, in turn, create particular chemical patterns in the stellar populations and their host galaxies.

It has long been known (Hoyle & Fowler 1960) that the explosion mechanisms, the chemical and energetic composition of the remnants and the light curves of SNeIa (with absence of He and H) involve, at the most fundamental level, the combustion of a degenerate stellar core. Specifically, a White Dwarf (WD) star of Carbon (C) and Oxygen (O) is lead away from the equilibrium, following mass accretion and successive explosion. Among the two most popular scenarios for explaining SNIa based on a thermonu-

clear explosion of a C-O WD, there is the Single Degenerate (SD) scenario – a WD exceeding the Chandrasekhar mass through accretion from a non-degenerate companion star– where the mass accretion can assume many configurations. The secondary star is proposed to be a Main Sequence star, a subgiant star, a helium star or red giant star (Whelan & Iben 1973; Iben & Tutukov 1984; van den Heuvel et al. 1992; Hachisu et al. 1996, 1999; Han & Podsiadlowski 2004; Geier et al. 2013). In addition to the variety of possible secondary stars, some models include other effects such as the metallicity dependence proposed by Kobayashi et al. (1998). The authors found that when the metallicity is lower than [Fe/H]< -1, the winds developed by the primary star (WD) accreting mass through the Roche lobe are too weak and the explosion cannot occur.

The second most popular scenario involving a thermonuclear explosion of a C-O WD is the Double Degenerate (DD) scenario – two WDs that loose angular momentum and energy by emitting gravitational waves and eventually merge. If the exceed the Chandrasekhar mass they ignite as SNIa (Iben & Tutukov 1984).

Other suggested theoretical scenarios include the "Collisional Scenario" where the head-on collisions of two WDs occurs instead of the spiralling due to loss of gravitational wave radiation. These collisions of two WDs of sufficiently large masses are predicted in dense environments such as globular clusters, and could explain supernovae occurring in the nuclei of galaxies (Lorén-Aguilar et al. 2010). On the other hand, the "Core-Degenerate (CD) scenario", where a WD merges with the core of an asymptotic giant branch (AGB) star and forms a rapidly rotating WD. This new configuration has a mass close to and above the critical mass for explosion, and was used recently as the best scenario to explain the observed properties of SN 2011fe (Soker et al. 2013). Additionally, the "Double Detonation" mechanism propose a sub-Chandrasekhar WD accumulating a layer of helium-rich material on the surface sufficiently massive and degenerate to cause a detonation (Shen et al. 2013). Finally, another type of Core-Degenerate scenario considered is the "super Chandrasekhar scenario". These models propose a Chandrasekhar or a super-Chandrasekhar mass WD formed in the planetary nebula phase (or at the end of the common envelope phase), from a merger of a WD companion with the hot core of a massive asymptotic giant branch (AGB) star (Tsebrenko & Soker 2013). However, a common characteristic of all these scenarios is that similar nucleosynthesis processes occur during the explosion creating mainly Fe. For a recent review on the SNIa progenitors see Maoz et al. (2013).

Lately, many empirical DTDs have been proposed. The Bimodal model by Mannucci et al. (2006) considers a DTD with two populations of progenitors of SNIa, one dominated by the "prompt" component that explodes within 100 Myrs after the formation of their progenitors, and the "tardy" component exploding on a wide period of time extending up to 10 Gyr . The shape of the bimodal distribution is given by the sum of two functions: a Gaussian centered at 5×10^7yrs, and an exponentially declining plateau function. Moreover, similar power law DTDs ($\sim t^{-1}$) have been recovered from different observational surveys. For instance, Totani et al. (2008) using field elliptical galaxies proposed such a power law. Maoz et al. (2012) also suggested a very similar DTD based on a sample of 132 SNeIa from the Sloan Digital Sky Survey II. Finally, Pritchet et al. (2008) presented a power law DTD ($\sim t^{-0.5}$) from the SuperNova Legacy Survey.

The DTD represents a powerful tool, not only for testing models and helping to constraint the progenitor SNIa scenarios, but also for obtaining an accurate description of the chemical and energetic feedback from SNIa. The aim of our work is to test which is the best scenario for SNIa in the framework of cosmological simulations. In particular, we will include and analyse in detail, for the first time to our knowledge, five different DTDs for SNIa in a smooth particle hydrodynamical code. Our results will be presented in a series of three papers.

In this first paper we will discuss in detail the SD model and compare our results, obtained for a bulge-type galaxy, with the chemical abundances and SNIa rates for this kind of galaxy. In particular, we will compare our results with the abundance data for the Milky Way bulge. We study global properties such as the correlation found by Sullivan et al. (2006) between the specific star formation rate (SSFR) and the specific SNIa rate (SSNIaR). The reason for starting with this par-

ticular scenario is that it has been suggested as one the best models to reproduce the chemical properties of galaxies (Matteucci et al. 2006, 2009).

This paper is organized as follows: Section 2 describes the analytic DTD for the SD scenario. Section 3 briefly describes the main aspects of the numerical code and presents the initial conditions. In the following Subsections we present the implementation of DTD in the code. In Section 4 we show the calibration of the model with the observables. In Section 5 we study the observed correlation found by Sullivan et al. (2006), between the specific SNIa rates and the specific SFR for the SD scenario. The main conclusions are summarized in Section 6.

2. The Single Degenerate scenario

In the SD proposed by Whelan & Iben (1973), SNIa originate from a binary system with one C-O WD and a red (super) giant star. The WD accretes mass from the red giant through the Roche lobe, and an explosive nucleosynthesis process occurs when the WD reaches the Chandrasekhar mass. Calculations of the SNIa rates were performed on the basis of this model (Greggio & Renzini 1983; Matteucci & Greggio 1986; Tornambe & Matteucci 1987; Matteucci et al. 2009) for both our Galaxy and for elliptical galaxies.

To calculate the SNIa rates in the framework of the SD scenario is necessary to know the range of lifetimes from the stars belonging to the exploding binary systems. One way to do this is to evaluate the minimum and maximum masses allowed for these systems, taking into account the fact that Type Ia SNe occur in all galaxies, including ellipticals which do not show any active star formation. In this work we adopt the model of Greggio & Renzini (1983, from now GR83), where the lifetimes of the stars exploding as SNIa are comprised in the mass range of $0.8 - 8 M_{\odot}$. Then, according to this mass range, after a starburst the first systems to explode as a SNIa (e.g. $8{+}8 M_{\odot}$ systems) will require no more than $\sim 3 - 4 \times 10^7$ yrs. And this is the most massive system possible with a total mass of $16 M_{\odot}$. On the other hand, the minimum mass possible for a binary system giving rise to a SN Ia explosion is estimated to be $3.0 M_{\odot}$ (see GR83). This total minimum mass

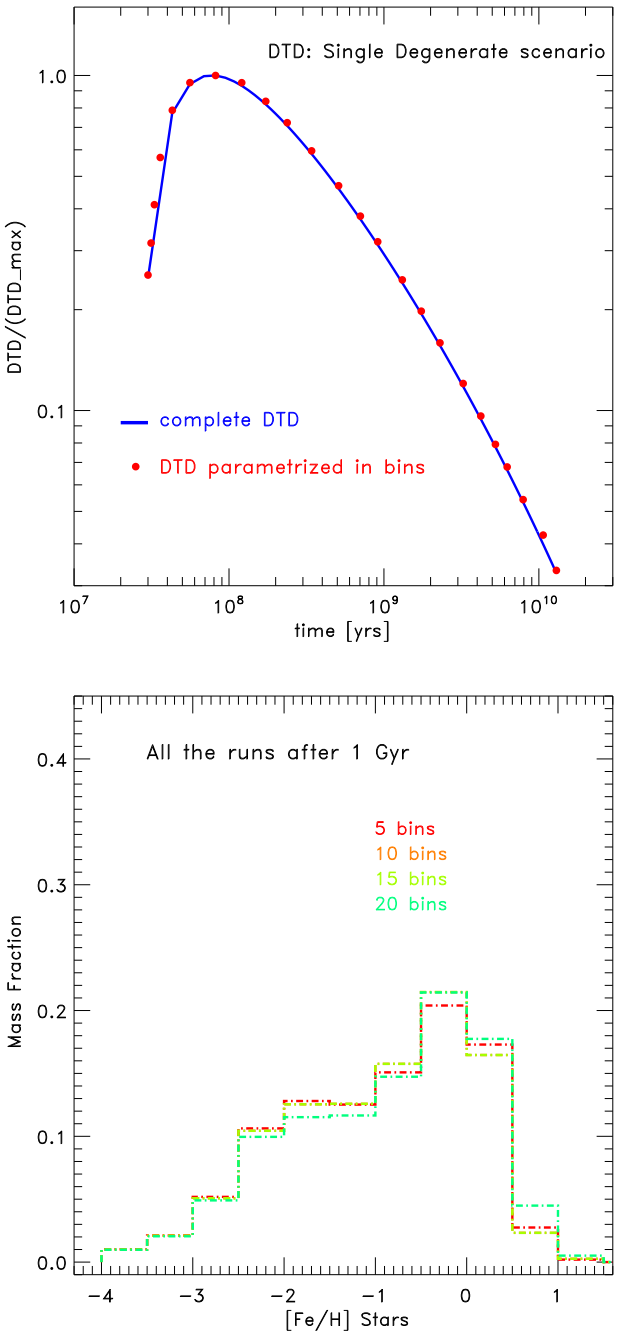


Fig. 1.— (*Upper panel*) The full DTD for the SD scenario given by Matteucci & Recchi (2001) and the DTD parametrized with 20 bins to reduce the computational costs (for more details, see the text). (*Lower panel*) Distribution of [Fe/H] ratios for the stars in the simulation, presented as an example of the relevant quantities of this study not being affected by the adopted number of bins used in the parametrization of the SD.

will ensure that the system can contain a white dwarf and a companion massive enough to allow the white dwarf to reach the Chandrasekhar mass after accretion.

For the calculation of the SNIa rates we follow the formulation of Matteucci & Recchi (2001, from now, MR01):

$$R_{\rm Ia}(t) = A \int_{M_{\rm B,inf}}^{M_{\rm B,sup}} \phi(M_{\rm B}) \int_{\mu_{\rm min}}^{\mu_{\rm max}} f(\mu)\psi(t-\tau_{M_2})d\mu\, dM_{\rm B}. \quad (1)$$

here $M_B = M_1 + M_2$ is the total mass of the binary system (where M_1 is the primary and M_2 the secondary). In the limits of the integral we use the minimum and maximum total masses for the binary systems ($M_{\rm B,inf}$ and $M_{\rm B,sup}$) described above. For more details see GR83 and MR01.

The only free parameter of this formulation is A, representing the fraction of binary systems able to produce SNeIa in the mass range 3-16$M_\odot$. This parameter is generally fixed by reproducing the present time observed SNIa rate of the type of galaxy under study.

In Equation 1, the function $\psi(t)$ represents the SFR. This quantity needs to be evaluated at the time $(t - \tau_{M_2})$, where τ_{M_2} accounts for the life of the secondary star. This constitutes the clock for the SNIa explosion (Padovani & Matteucci 1993). The function $\phi(M_B)$ refers to the Initial Mass Function (IMF) from Salpeter (1955), defined in the mass interval 0.1-100 $M_\odot$, with an index of $x = 1.35$.

$$\phi(M_{\rm B}) = C M_B^{-(1+x)} \quad (2)$$

The mass fraction of the secondary star to the total mass of the system is the quantity $\mu = M_2/M_{\rm B}$, and its distribution function is given by $f(\mu)$. Previous studies (Tutukov & Yungelson 1980) suggest a value of γ=2, that we also adopt here, as previously used in the formula:

$$f(\mu) = 2^{1+\gamma}(1+\gamma)\mu^\gamma. \quad (3)$$

It is worth noting that the integral in Equation 1 when computed without the SFR, namely for an instantaneous starburst, is the so-called Delay Time Distribution (DTD) function (shown for the SD in top panel of Figure 1).

This approach allows us to evaluate the Equation 1, for each stellar particle with a SF episode and estimate the rate of SNIa.

3. The numerical code

We use an extended version of the Tree-PM SPH code GADGET-3 (Springel 2005), which includes metal-dependent cooling (Sutherland & Dopita 1993), star formation, chemical enrichment, supernova feedback (SN), and a multiphase model for the gas component (Scannapieco et al. 2006). In this scheme if two gas particles have dissimilar thermodynamic properties, they are explicitly prevented from being neighbours in the SPH calculations (unless they are in a shock), allowing the coexistence of gas clouds with different thermodynamical properties. The SN feedback scheme is coupled adequately with the multiphase model. As a result, the energy injection into the ISM produces the self-regulation of the SF and the triggering of mass-loaded galactic outflows. This SN feedback does not introduce mass-dependent parameters as described in detail by Scannapieco et al. (2006). In this work, we assume the total SN energy release in each event to be 0.7×10^{51} erg and is equally distributed within the cold and hot phases surrounding a stellar particle. Our SN feedback model has already been used to study the formation of disc galaxies in a cosmological context (e.g. Tissera et al. 2013b,a; Artale et al. 2015).

The cold and dense gas is transformed into stars when satisfying density and temperature criteria according to the Kennicutt-Schmidt law (Schmidt 1959; Kennicutt 1998). We adopt a Salpeter IMF, defined in the mass interval of 0.1-100 $M_\odot$. SNe type II are assumed to originate from stars more massive than M> 8 $M_\odot$and lifetimes of $\sim 10^6$ yrs.

The SNIa prescription included in Scannapieco et al. (2006) was originally proposed by Mosconi et al. (2001). Regarding the SNIa implementations, the model of Scannapieco et al. (2006) will be referred as the "original model" to distinguish it from the new implementations for the SNIa (based on different DTDs), presented in this and the following papers. In the original model the lifetimes of the binary system that explode as SNIa are assumed to be randomly

distributed within a certain range given by $\tau_{SNIa} = [0.1, 1]$ Gyr [1]. This SNIa scenario, albeit simple, has been successful at reproducing many observational chemical patterns and trends as shown in Tissera et al. (2012, 2013b, 2014). The original model has the large advantage of being computationally inexpensive while grafting the main features of SNIa. However, there is room for improving the SNIa modeling as explained in the Introduction. This would be of a great importance when large on-going or planned surveys of the our Galaxy or nearby galaxies start to yield detailed abundances of the stellar populations such as APOGEE (a part of the Sloan Digital Sky Survey III) (Anders et al. 2013), The GIRAFFE Inner Bulge Survey (GIBS) (Zoccali et al. 2014), The Calar Alto Legacy Integral Field Area (CALIFA) survey (Sanchez et al. 2013), The Sydney-AAO Multi-object Integral field spectrograph (SAMI) (Croom et al. 2012), among others.

3.1. The simulated galaxies

We analyse the performance of the DTDs in simulations of pre-prepared galaxies in isolated dark matter haloes. This initial condition (IC) is simple enough to highlight the effects of the different DTDs without being distracted by additional processes such as mergers and gas infall, which complicate the picture in fully hierarchical scenarios for galaxy formation. This simple approach allows us to more easily test the influence of the free parameter of the implemented DTDs.

The IC consists of a dark matter potential with an initial distribution following a NFW density profile (Navarro et al. 1997), which is let to evolve self-consistently with the baryonic component, with a concentration of $c = 9$, an old stellar bulge with a Hernquist profile and a old stellar exponential disc. The virial mass of this system is $M_{200} \sim 10 \times 10^{11}$ $M_\odot$, with 10% of this mass in form of baryons. The adimensional spin parameter is $\lambda = 0.044$.

Initially, the gas is distributed in the disc component and represents $\sim 65\%$ of the total baryonic mass of the galaxy. Within the total disc component, the gas represents a fraction of $\sim 90\%$ of the initial mass of the disc. This initial large gas fraction has been chosen to mimic a galaxy in its first stages of evolution in a simple way. At the beginning of the simulations the disc component is in equilibrium within the potential well ($Q > 1$) and has a scale-length of ~ 3.4 kpc. The gaseous disc has a lower Q value (closer to ~ 1) and becomes unstable developing clumps and bar instabilities. These two perturbations transport material into the inner regions of the galaxy contributing to the formation of the bulge component. In particular, the bar drives gas inflows which trigger important starbursts (for more details see Perez et al. 2011, 2013).

In all the simulations the initial number of baryonic particles is ~ 80000 and the dark matter particles ~ 100000. Specifically, the initial gas particle is $\sim 7 \times 10^5$ $M_\odot$ while the dark matter particle is 9×10^6 $M_\odot$ and the stellar mass particle, $\sim 3 \times 10^5$ $M_\odot$. The softening length for the gas particles is 200 pc and for the dark matter particles we adopt 450 pc. The SFR efficiency is set at $c = 0.1$. We follow the evolution of the systems until the gas to form stars is depleted and the star formation ceases.

We decomposed the bulge and disc components of the simulated galaxies by adopting a dynamical criterion based on the ratio between the rotational and dispersion velocities (e.g. Scannapieco et al. 2008). From this analysis we identify a bulge and disc component. The bulge is formed by a dissipative-dominated component and a central bar. The stellar density profiles show that the bulge is concentrated within the inner ~ 3 kpc. This configuration shows a ratio of $B/T \sim 0.84$. Hence, the new stars formed for which we follow the chemical abundances are mainly part of the bulge.

Even more, the analysis of the SFR of the bulge shows that the stars formed during the strong starbursts, where the cold gas is exhausted within ~ 1 Gyr. The new stars remain concentrated within ~ 3 kpc. All the simulations show this strong ini-

[1] These limits can be varied as has been done by Scannapieco et al. (2009) in the Aquarius simulations, for example, thus considering a larger minimum lifetime for the distribution of the secondary mass, compared to the predictions of the SD scenario. This constitutes a simple approach based on the assumption that a fair fraction of SNIa will explode during a period $\tau_{SNIa} = 10^8 - 10^9$ yrs (Greggio 1996). A fixed relative ratio between SNII and SNIa is assumed adopting an observationally motivated value (van den Bergh 1991), which can be associated with the free parameter A. The chemical yields in all the models are give by the W7 model of Iwamoto et al. (1999)

tial SF burst ending before ~ 1 Gyr due to the gas depletion into stars, and the effects of SN feedback which ejects part of the gas (see Subsection 4.1). The B+D stellar mass is nearly the same for all the simulations $\sim 3.5 \times 10^{10}$ $M_{\odot}$, typical of a small ellipticals or spiral galaxy bulges.

By comparing these SF histories with the ones given by the model of Pipino & Matteucci (2004, hereafter PM04), we conclude that the SF history of the gas component resembles spheroidal-type systems. This is consistent with the fact that the gas becomes unstable and collapses into the central region, feeding the strong starbursts. Most of the new stars are centrally concentrated, contributing to the formation of the bulge component. Therefore, we compare the present day SNIa rates with those observed in spheroidal-dominated galaxies. The chemical patterns will be confronted with observations of the Galactic Bulge as these are the only observations available of individual stars in a bulge. We do not attempt to reproduce exactly these data since the formation history of the Galactic Bulge seems to be more complicated (Rojas-Arriagada et al. 2014), but to use the data to set global constrains on the A parameter.

3.2. Implementation of the DTD

The numerical code estimates whether if a given gas particle meets the condition to be transformed into stars. Then, the code follows over time the new stellar particle, representing a single stellar population, and calculates the number of SNIa which should be produced as a function of time, according to the assumed DTD. The free parameter A is adjusted to reproduce the present-time observed SNIa rates. Analytical or semi-analytical models fix the value of A requiring the galaxy to reproduce the observed SNIa rates according to its morphology. In a numerical simulation, A is tuned at a particle level, so a given stellar particle does not have any a *priori* knowledge of the morphology of the galaxy it inhabits. On the contrary, reproducing the observed SNIa rate according to morphology should be a prediction of our models. Note that in our models, gas and star particles will evolve according to the physical laws in a non-linear way. Hence, reproducing the observed values is a challenge, even with a IC as simple as the one adopted in this work.

Table 1: Main characteristics of the simulated galaxies run with the SD scenario and varying A. The mean observed SNIa rate for spheroidal dominated galaxies of stellar mass $\sim 3.5 \times 10^{10}$ $M_{\odot}$is ~ 0.0017 SN per year (Li et al. 2011).

Model	A	<SFR>	SNIa rates
		$[\ M_{\odot} yr^{-1}]$	$[N/yr^{-1}]$
SD-1	0.0015	83	0.002
SD-2	0.00015	60	0.00006
SD-3	0.0075	84	0.0080
SD-4	0.00075	76	0.0016
original	0.0015	53	0.0027

As mentioned in the Introduction, there are several theoretical scenarios for the DTDs. This paper considers the SD by MR01 and leave for Paper II the following scenarios: DD by Greggio (2005), the Bimodal scenario by Mannucci et al. (2006), the power laws proposed by Maoz et al. (2012), and by Pritchet et al. (2008). The implementation of the DTDs is the same for all the models.

The drawback of including detailed descriptions of the DTDs in the simulations is the computational cost for our particular SN feedback model. The objective is indeed to keep the model running efficiently to allow its use in large-scale cosmological simulations. Therefore, solving the integrals given by Equation 1 for each particle, at each time, is highly inefficient. This is related to the methodology followed by SN feedback model. In the adopted scheme, the code has to search for the nearest hot and cold gas particle neighbours of a given stellar particle in order to inject the energy and chemical elements. This procedure is very time-consuming. To alleviate this problem, we include the DTDs in the simulations by creating tables for each DTD. We use 20 equally time-spaced bins to parametrize the complete DTD distributions. This can be visualized in the upper panel of Figure 1, where we show the complete DTD for the SD scenario given by MR01 (continuous line), and the re-sampling with 20 intervals or bins (red dots). The representation of the DTD with a this lower number of intervals reduces the computational costs by limiting the hot and cold neighbours searchings required to inject the SNIa products, without losing the relevant information

stored in the complete DTD distribution. The SNIa rates for each stellar particle (i.e. representing a single stellar population) are estimated by searching in the DTD table for the number of SNIa which should be produced according to the particle stellar age and the adopted progenitor model. Then, the total SNIa rates for the central spheroid are calculated by adding the contributions form each star particle identified to belong to this component. In particular, we use the rates at the time when the SFR is quenched to compare with other models and observations. Thanks to this efficient implementation based on pre-prepared tables for the DTDs, the computational costs are significantly reduced.

We study the convergence of different parametrizations of the DTDs varying the bins numbers used to map the DTDs. We run the SD-1 model with $[5, 10, 15, 20]$ number of bins for fitting the DTD curve, finding that the distribution of metals, the SFR, specific SFR, the SNIa rates, and other relevant quantities for this study do not not change significantly with the number of bins chosen. To illustrate this fact we show in the right panel of Figure 1, histograms of the mass fraction of stars within a given [Fe/H], calculated for models with different numbers of bins. It can be seen that the differences between the fractions of mass are negligible. Notice, for example, that the fraction of stars with [Fe/H]> 0 vary less than 0.2% between the models.

4. Calibrating the SD scenario

Chemical evolution models calibrate the DTDs using the free parameter A fixed a *posteriori*, to fit the present day observed rate of SNIa. This parameter accounts for the fraction of binary systems that undergo a SNIa event in a starburst once the IMF is fixed. In the SPH simulations A is also a free parameter but on particle basis. Thus is not possible to know *a priori* in which morphological type of galaxy a given particle inhabits, particularly in a cosmological simulation. The parameter A has to reflect the underlying physics and, at the same time, be able to reproduce the mean observable constraints.

To explore the range of A values able to reproduce observations, we make use of the multi-zone chemical evolution model of PM04 for bulge-like systems of similar mass and SF history as the SPH galaxies. Once we find a parameter space for A, we run the SPH simulations. The advantage of this methodology is the small computational cost of running the multi-zone chemical evolution model of PM04, compared to the cost of running several SPH simulations until selecting the proper values for A. Caution should be taken since a change in A might produce a non-linear response in the SPH simulations, as the SN feedback and gas metallicities will also change, modifying the cooling rates and the availability of cold gas for subsequent star formation activity.

Specifically, in the PM04 model a galaxy is divided into several non-interacting shells. The chemical evolution equations are solved in each shell in order to reproduce the evolution of the elemental abundances. The SFR is given by the law $\psi(t) = \nu\rho_{gas}(t)$, assumed to be proportional to the gas density ρ_{gas}, via a constant ν, representing the star formation efficiency. This quantity in the PM04 models increases with the baryonic galaxy mass. For the comparison with the SPH simulations, we run the model of PM04 adopting $\nu = 50$ Gyr^{-1} for a galaxy with initial mass of 10^{11} M$_\odot$and a infall time of 0.01 Gyr. Because of the stellar winds suffered through its evolution, the galaxy ends up with a final mass of $\sim 4.7 \times 10^{10}$ M$_\odot$. And this mass is of the order of magnitude of the new stellar mass formed in the SPH galaxies ($\sim 3.5 \times 10^{10}$ M$_\odot$). The SFR history of the SPH galaxies and the PM04 galaxies are very similar, showing a bursty behaviour at the beginning with a fast quench after ~ 1 Gyr. These SFRs are shown in Figure 3, upper panel.

The following step is to use the SFR of the SPH galaxy obtained running the original model of Scannapieco et al. (2006) as an input to the model of PM04. In this way, we obtain a prediction for the rates of SNIa and SNII for the given galaxy. By varying the value of A in the PM04 model, we can find the adequate parameter space for A. This parameter space is then the one we adopt in the SPH simulations. As a constraint to our models we use the rate-size relation of Li et al. (2011) and derive the observed SNIa rate at the present time, following the method shown by Valiante et al. (2009). We do this for a galaxy with baryonic mass similar to our simulated galaxy. Thus, for a system of $\sim 3.5 \times 10^{10}$ M$_\odot$,

the rate predicted by Li et al. (2011) is ~ 0.0017 SNIa per year.

We run four experiments with the same IC and the SD model using A $= [0.0015, 0.00015, 0.0075, 0.00075]$ (SD-1, SD-2, SD-3 and SD-4 models). Larger or smaller values are strongly ruled out by the PM04 model. Table 1 summarizes their main properties, including the predicted SNIa rates (column 4), calculated when the SFR is quenched. It can be seen that we obtain good agreement with SD-1 and SD-4. The original model, with $A = 0.0015$, also reproduces the observed SNIa rates.

The behaviour of the SNIa rates as a function of time for the different models is shown in Figure 2. It becomes clear from the plot that not only the A parameter affects the rates, but also the lifetimes of the progenitor systems that explode as SNIa given by each model. Recall that for the SD scenario the first systems made of two $8M_{\odot}$ stars explodes after $\sim 3 - 4 \times 10^7$ yrs after the starburst. On the other hand, for the original model the lifetimes are assumed to be randomly distributed within a certain range given by $\tau_{SNIa} = [0.1, 1]$ Gyr. Thus, the predicted rates for the original model are delayed in time relative to those of the SD, and lacking of the prompt SNIa (those exploding in the first 0.1 Gyrs), as can be seen in Figure 2. In the following section we analyze the consequences of this delay in the SFR.

4.1. Star Formation Rate

In Figure 3 (upper panel), we show the SFR of the simulated galaxy for all the explored A values. The SFRs are estimated by using constant time intervals along the history of the galaxies. In all the runs, there is strong burst at the beginning, followed by a decay of the SFR until the gas is exhausted. Since the simulated galaxy is isolated, there is no external gas reservoir to keep feeding the SF. No meaningful differences between the models appear until the SFR declines below ~ 10 M$_{\odot}$yr^{-1}. The SFR for the SD-1 model is the first to drop to ~ 0.01 M$_{\odot}$yr^{-1} after $\sim 4 \times 10^8$ yrs. The model SD-2, with the lowest A value, is the last to exhaust the gas by forming stars after $\sim 8 \times 10^8$ yrs. Models SD-1 and the original share the same value of A but show different quenching times. The latter being the one with more extended SFR. All the simulations have their SFR quenched before 1 Gyr, due to gas depletion into stars and/or the effects of SN feedback, which heats up part of it.

Alternatively, we quantify the effects of the parameter A acting on the regulation of the SF by the estimation of the mass fraction of new-born stars. Figure 3 (lower panel) shows clearly how different A can regulate the SF activity according to the total energy that SNeIa inject into the ISM. The efficiency of the stellar production depends on the available cold gas in galaxies, a quantity linked to the number of SN events occurring in the galaxy. From Figure 3 we can see that when the value of A increases the fraction of new stars decreases accordingly. This can be clearly appreciated from the comparison between the final fractions reached in SD-3 and SD-2, with the highest and lowest values of A, respectively. However, the variations between models are very small (less than 2%) indicating that, at least for this IC, the effects on the regulation of the SF are minor, if sensible values of A are assumed.

Comparing the original and SD-1 models we can see that they produce the same fraction of new-born stars, although the star formation activity is quenched earlier in the SD-1 model. Recall that in the SD model the minimum lifetime of SNIa is $\sim 3 \times 10^7$ yrs, whereas in the original model is $\sim 1 \times 10^8$ yrs (see Figure 2). This explains the differences in the SFR quenching times of the two models. Notice that the DTD implementation seems not to affect the efficiency of the fraction of new-born stars formed in the galaxies when compared to the original model. Observational evidence of the existence of prompt SNeIa strongly argues in favour of a minimum time-scale as long as $\sim 10^8$ yrs (Bonaparte et al. 2013, and references therein).

Notice that even when the SNIa can continue to pollute the ISM with the nucleosynthesis production after the SFR has stopped, this will not affect the chemical abundances of the stellar populations since no new stars will be formed from the enriched gas. Therefore, in the following Section we analyse the distribution of chemical elements at this particular time: when the SFR is quenched. Analytical and multi-zone chemical evolution models adopt a similar criterion that we also chose here for the sake of comparison.

4.2. The [O/Fe] vs. [Fe/H] diagram

We study here the predicted [O/Fe] vs. [Fe/H] relation by each of the models of the SD scenario included in the SPH simulations. It is worth remembering that the parameter A is tuned to reproduce the present time observed SNIa rate. In our case, the values of A which best reproduce the present time rate are those of SD-1 and SD-4 models, as already shown in Section 4. Here we test the effect of varying A, namely the fraction of SNIa, on the predicted [O/Fe] ratios.[2]

We interpret the evolution of the abundance ratios of [O/Fe] vs [Fe/H] with the help of the time-delay model of Tinsley (1979). It is expected that the delay in the production of Fe by SNIa ejected into the ISM – in relation to the rapid production of α elements by SNII – leaves a characteristic signature in the [O/Fe] vs [Fe/H] diagram MR01. The ejection of Fe from SNIa is regulated by the DTD. The main effect of the delayed Fe production in relation to the α-elements produced by SNII, is to create an over-abundance of α-elements. In particular, the Oxygen remains high until SNIa becomes important and the ratio [O/Fe] starts to decline. This point is identified by a "knee" in [O/Fe] vs [Fe/H] diagram (see Figure 4).

Assuming that bulges and elliptical galaxies experience a strong burst of star formation lasting a short time (less than 1 Gyr) Matteucci & Brocato (1990a) predicted that [α/Fe] should be supersolar for a large interval of [Fe/H]. In fact, objects such as bulges that evolve very fast with an intense SFH, quickly reach solar metallicity only due the production of Fe by SNeII. When SNeIa start to explode, the production of Fe is enhanced and a change in the slope (the knee) in the [O/Fe] vs [Fe/H] diagram occurs at [Fe/H] ≥ 0.

We compute the average stellar mass abundance of [Fe/H] and [O/Fe] for the stars in the bulge (see Sec. 3.1), for each of the models. The ratios [Fe/H] and [O/Fe] are calculated by adding the masses of the corresponding chemical elements stored in the star particles identified to belong to the central spheroid. We show the SD models with different values of A in Figure 4, where the different coloured lines refer to each of the models compared to Galactic Bulge stars. A sample of dwarfs and subgiant stars from Bensby et al. (2013), and Red Giants stars from Lecureur et al. (2007), are considered for comparison.

Figure 4 shows the observed data points lying in between the curves displayed by models SD-3 and SD-2, corresponding to the highest and lowest values of A, respectively. However, model SD-2 predicts a too flat [O/Fe] ratio. This means that the fraction of SNIa is too low. On the other hand, model SD-3 is an extreme case where there are too many SNeIa and it predicts, in fact, a continuous decrease of the [O/Fe] ratio, at odds with the observations. The data are best represented by the models SD-4 and SD-1. The former model (SD-4) fits the zero point of the data following the observed trend up to [Fe/H]~ -0.25. Meanwhile, SD-1 matches the slope and passes through the data better. These models predict a long plateau for the [O/Fe] ratio and a knee occurring at high [Fe/H], as observations suggest. However, as can be seen in the Figure 4, at high metallicity the slopes of both models do not so nicely follow the observed [O/Fe] ratios. This is perhaps a consequence of yields adopted in this work. The WW95 yields do not include mass loss from massive stars, which is particularly important for Wolf-Rayet stars and for supersolar metallicity. Its effect is to increase the yields of Carbon and Helium and to depress that of Oxygen, as extensively described in McWilliam et al. (2008). Notice that SD-1 and SD-4 models also fit the present time SNIa rates (see Section 4). The original model, albeit simple, fits the data in the whole range.

From the previous analysis, we conclude that the chemical enrichment shown by the [O/Fe] ratios changes linearly with A in the SD scenario. Therefore, it is possible to find a range of values of A which can predict the current SNIa rates and the expected trend for [O/Fe] ratios at the same time. It also shows the importance of calibrating the models using observables.

The [O/Fe] vs [Fe/H] ratios observed in the solar neighbourhood had been reproduced for Milky Way-type (MW) galaxies by several galaxy formation models (e.g. Calura et al. 2012; Yates et al. 2013; Few et al. 2014; De Lucia et al. 2014), although some of them fail to reproduce the most

[2] In the original and SD models the yields used for SNeII are those metal-dependent from Woosley & Weaver (1995). For the production of SNIa, we assume the W7 model by Iwamoto et al. (1999).

enriched starts for the MW bulge, showing an offset with the data (see for example Figure 12 from De Lucia et al. 2014).

The "knee" of the bulge shown in Figure 4 occurs around [Fe/H]~ -0.25, at variance from the observed value for the disc component of the Milky Way found at [Fe/H]~ -1 (François et al. 2004). This difference is a consequence of the strong SF experienced by the spheroidal component, making it evolve faster than the disc. As a result, it reaches higher values of [Fe/H] at the time when the SNeIa stars to become important and restore the bulk of Fe to the ISM (a prediction from chemical evolution models Matteucci & Brocato 1990b). Therefore, we recall the reader than the time-scale for the SNIa reaching its maximum enrichment, usually quoted as ~ 1 Gyr, is not universal but only valid for the solar neighbourhood, as can be seen in this example and was pointed out by MR01.

5. The correlation between the SNIa rates and the specific SFR

Observations relating the SNIa rates of galaxies with the characteristics of the host galaxy such as their morphology, colours and SFR are powerful constraints to our models. Consequently, in this Section we compare the results of the best SD scenario with observations presented by Sullivan et al. (2006). In that paper, the authors found a correlation between the Specific Star Formation Rate (SSFR) – the SFR per unit mass of the galaxy –, and the specific SNIa (SSNIa) – the rate of SNIa per unit of galaxy mass – for galaxies in the SuperNova Legacy Survey (SNLS) galaxy sample. This correlation is based on a sample of 100 spectroscopically confirmed SNeIa, plus 24 photometrically classified events, distributed over $0.2 < z < 0.75$. The stellar masses and SFRs for the SNIa host galaxies are estimated by fitting their broadband spectral energy distributions (SEDs) with the galaxy spectral synthesis code PEGASE.2 (Fioc & Rocca-Volmerange 1997). They adopt the IMF of Kroupa (2001). The SSFR for the sample is measured as the ratio between the mean SF rate over the last 0.5 Gyr and the current stellar mass of the galaxy, resulting from the SED fitting. They choose this interval of time to avoid systematic errors for galaxies for which the redshift is not known.

Furthermore, Sullivan et al. (2006) compared the correlation with observations of a morphologically classified sample of SNeIa host galaxies in the local universe presented by Mannucci et al. (2005). It became clear from this comparison that the sample of galaxies in the local universe shares the same trend displayed by SNLS galaxies at higher redshift. Therefore, the SSNIaR is a function of the host galaxy SSFR, with strongly star-forming galaxies hosting roughly 10 times as many SNeIa per unit mass than passive galaxies with no star formation.

Moreover, Smith et al. (2012) obtained the SNIa rates of galaxies with different SFR activity located at intermediate redshift ($0.05 < z < 0.25$), from a sample of 342 galaxies belonging to the Sloan Digital Sky SuperNova Survey-II (SDSS-II SN Survey). The authors estimated the host stellar masses and the recent star-formation rates using the code PEGASE.2. They confirmed the existence of a correlation between the SSFR and the SSNIaR. Therefore, the correlation holds for intermediate redshifts (Sullivan et al. 2006), and for the local Universe (Mannucci et al. 2005), indicating no evolution with redshift within the range of $0.05 < z < 0.75$.

Sullivan et al. (2006) concluded that the correlation is difficult to reconcile with a model for SNIa that originates solely from an old evolved stellar population. Instead, they proposed a scenario of two separate components: a prompt component with a short delay time and an old component with a long delay time, consistent with the Bimodal model of Mannucci et al. (2006). Here we explore this relation with the SD model and in Paper II the analysis will be extended to the other DTD models.

To assess if our best SD models are able to reproduce a correlation such as the observed one, the SSNIaR and the SSFR are estimated as the galaxy evolves, under the hypothesis that observations might catch galaxies at different stages of evolution (see also Figure 12 in Greggio (2010) for a similar approach using analytical models). For this purpose, we calculate the SSNIaR and the SSFR of the simulated galaxies as a function of time. This is done by using the SFR histories and the SNIa rates of the simulated galaxies and their corresponding stellar masses as function of time

(e.g. Figure 3). These quantities allow us to calculate the mean SSFR and SSNIaR at different stages of the galaxy evolution. The averages over the whole stellar population are taken at a certain period of time, chosen to be within 0.5 Gyr, in order to mimic observations. [3] Smith et al. noticed that the zero point of the correlation is affected by the choice of the IMF, systematic uncertainties concerning the accuracy of the derived properties of host galaxies and the photometric redshift estimates produced by PEGASE SED fitting code. Therefore, because of all these uncertainties, we focus on the study of the slope of this correlation and prefer not use the error bars provided by the observational works. Consequently, the simulated relations are normalized by an *ad hoc* factor to simplify the qualitative comparison of the observed slope of the correlation.

A combination of the observed data by Smith et al. (2012); Sullivan et al. (2006); Mannucci et al. (2006), and the results for the SD-1 and SD-4 models are shown in Figure 5. Although a word of caution is necessary when making comparison between the evolution in time of single objects – like our simulated galaxies – and observations referring to a mix of different objects that might have undergone different evolutionary histories, it is interesting that our model including the SD scenario reproduces a clear correlation which agrees remarkably well with observations.

As can be seen from Figure 5, at the beginning the simulated correlations follow a different trend, so that the SSNIaR increases abruptly to high values of SSFR before reaching the expected observed trend. This feature is detected for all A values in the SD model, as can be seen in models SD-1 and SD-4. These strong variations in the SSNIaR are produced in a short interval of SSFR for most of the models ($8.5 < \log \mathrm{SSFR} < 7.5$) and are related to the time-delay in the SNIa explosions.

To understand the physical reasons causing the SSFR-SSNIaR correlation, we plotted the logarithm of SSFR and the SSNIaR as a function of time for the SD-1 and SD-4 models in Figure 6. The sharp increase of SSNIaR for high SSFR reflects the onset of SNIa and how quickly it reaches the maximum value. After that, both the SSNIaR and the SSFR decrease establishing the observed correlation. For very low SSFR, there is still a residual SSNIaR, as the generation of these events is delayed in time and the correlation is lost.

The particular feature seen at the beginning of the SSFR-SSNIaR relation is not shown by the current observational data and represents a prediction from the simulations. If these early stages could be observed, then they could be used to set limits on the shape of the DTDs. Of course, the system we have used to explore the effects of varying the DTDs is very simple. The SF history of galaxies could certainly be more complicated with several starbursts occurring during their life. The analysis of these complex stellar populations is delayed to a forthcoming paper using cosmological simulations.

6. Discussion and Conclusions

We present results from simulated galaxies performed with a version of Tree-PM SPH-GADGET-3 (Springel 2005; Scannapieco et al. 2006), to study the impact of the SNIa feedback by using different DTDs. In this paper, we explore the SD model of MR01 in detail. We choose the SD scenario as a reference to discuss the implementation, the main observables and correlations which we aim to reproduce. The implementation of the SD scenario involves the calibration of a free parameter A which represents the fraction of binary systems in one stellar generation giving rise to SNIa events. Chemical evolution models generally fix A according to the SFR and the present day SNIa rates of the galaxy under study. However in a cosmological simulations A acts at a particle basis. Thus, it is assumed to be the same for all single stellar populations, while the final SNIa rates or any relation between the SNIa rates and the galaxy properties – or the chemical abundance patterns – should come out as a prediction of the simulations. Therefore, it is necessary to explore a range of suitable A values and their impact on the properties of galaxies, by using simple initial conditions. In a forthcoming paper, we explore other progenitor scenarios. The final goal is to run cosmological simulation and analyse the chemical properties of galaxies of different masses and assembly histo-

[3] To correct for the different IMFs used in this work (Salpeter) and the observations (Kroupa), we adopt the transformation suggested by Longhetti & Saracco (2009).

ries. Adequately reproducing the SNIa feedback as well as their effect on the chemical enrichment is very important, as new Galactic surveys will start yielding high precision measurements of chemical abundances.

Our main results can be summarized as follows:

- We find that the SFR responds linearly to the number of SNeIa in the SD scenario. The SFR is found to decline faster with increasing values of A. But the differences are small and so the final stellar mass formed is very similar. There is a substantial difference between the original model of Scannapieco et al. (2006) and the SD of Matteucci & Recchi (2001) implemented and analysed here. This is related to the adopted lifetimes for the secondary masses. In the original model, the SNIa production was shifted to later times, compared to the SD scenario, beginning at $\sim 1 \times 10^8$yrs. This excludes the so-called prompt SNeIa, that are indeed observed. For a similar A, the original model shows a more extended SFR. However, both of them predict similar final fractions of new stellar mass to total baryonic mass.

- The SFR in the simulations is dominated by a strong starburst consuming the cold gas within ~ 1 Gyr and forming stars that end up concentrated within the bulge. Hence, the SNIa rates are comparable to observed ones for spheroidal galaxies. This comparison with observed SNIa rates of Li et al. (2011) shows that the best fits are obtained for SD-1 and SD-4 models, adopting A~ 0.0015 and A~ 0.00075, respectively.

- The [O/Fe] ratios predicted for the stars in the bulge of the simulated galaxies are compared to data from the Galactic Bulge (although this comparison is just indicative). We find that the best agreement with observations is again provided by the SD-1 and SD-4 models. These models predict a long plateau for the [O/Fe] ratio and a knee occurring at high [Fe/H], as observations suggest. We note that this is the first time that such an excellent agreement is found in galaxy simulations.

- At variance with previous claims, we find that the SD scenario (SD-1 and SD-4 models) reproduce the observed correlation between the SSNIaR and the SSFR, found by Sullivan et al. (2006), if we estimate these quantities at different evolutionary times. This correlation comes out naturally from the simulations. Moreover, two features in the correlations are shown which cannot be confronted with current observations but could be interesting to explore in the future:
  - 1) For high SSFR, as the SSNIaR starts to appear, the SSNIaR-SSFR anti-correlates before it turns into the observed correlation. This is caused by the large initial number of SNe Ia in the assumed DTD. The turnover occurs when the maximum in the DTD is reached and hence, it could be interesting to explore if this turn-over could be confirmed with observations coming from galaxies dominated by a very recent starburst.
  - 2) For very low SSFR, there is still a residual SSNIaR because the majority of these events are delayed in time, thus the correlation disappears. The SSFR at which this occurs could be related to the shape of the DTD.

In a forthcoming paper, we will discuss other DTDs implemented in the SPH simulations: the DD scenario by Greggio (2005) and empirically motivated DTDs such as the Bimodal scenario by Mannucci et al. (2006), the power laws reported by Maoz et al. (2012) and Pritchet et al. (2008). We will explore the predicted SNIa rates and chemical abundances, as well as the global correlations which can contribute to the understanding of SNeIa progenitors.

Acknowledgments

NJ is very grateful for fruitful discussions and comments from Marcelo Miller Bertolami, Ilaria Bonaparte, Emanuele Spitoni, Laura Greggio,

Jordi Isern, Nikos Pranzos, Robert Yates, Manuela Zoccali, Thomas Bensby, Enrique Gaztaniaga, Emanuel Sillero and Kai Hoffmann. Many thanks to Kate Rowlands, Jack A. Kennedy for their comments and corrections to the manuscript. We thank the anonymous referee for a very constructive report that helped to clarify the paper.

We thank Mark Sullivan and Mathew Smith for kindly providing the data shown in this paper.

NJ acknowledges support from CONICET-Argentina; the European Research Council Starting Grant (SEDmorph; P.I. V. Wild); the European Commission's Framework Programme 7, through the Marie Curie International Research Staff Exchange Scheme LACEGAL (PIRSES-GA-2010-269264) and warmly thanks the Observatory of Trieste and the Institute of Space Studies of Catalunya, where most of this work was done.

This work was partially supported by PIP 2009/0305(CONICET-Argentina) and PICT Raices 2011/959 (Foncyt-Argentina). Simulations where run in Fenix Cluster of Institute of Astronomy and Space Physics (IAFE-Argentina) and Hal Cluster of the Universidad Nacional of Cordoba (Argentina). Also, this work was supported by PIP 2009/0305(CONICET-Argentina), PICT Raices 2011/959 (Foncyt-Argentina), "Proyecto Interno" of the Universidad Andres Bello (Chile), and Fondecyt Regular 2015 1150334. F.M. acknowledges financial support from PRINMIUR2010-2011, project: "Chemical and dynamical evolution of the Milky Way and Local Group Galaxies", prot.N. 2010LY5N2T. This research made use of the NASA's Astrophysical Data Systems and arXiv.org e-print service from the Cornell University.

REFERENCES

Anders, F., Chiappini, C., Santiago, B. X., et al. 2013, ArXiv e-prints, arXiv:1311.4549

Arrigoni, M., Trager, S. C., Somerville, R. S., & Gibson, B. K. 2010, MNRAS, 402, 173

Artale, M. C., Tissera, P. B., & Pellizza, L. J. 2015, ArXiv e-prints, arXiv:1502.00017

Aumer, M., White, S. D. M., Naab, T., & Scannapieco, C. 2013, MNRAS, 434, 3142

Bensby, T., Yee, J. C., Feltzing, S., et al. 2013, A&A, 549, A147

Bianchi, S., & Schneider, R. 2007, MNRAS, 378, 973

Bonaparte, I., Matteucci, F., Recchi, S., et al. 2013, MNRAS, 435, 2460

Bravo, E., Isern, J., & Canal, R. 1993, A&A, 270, 288

Calura, F., & Menci, N. 2009, MNRAS, 400, 1347

Calura, F., Gibson, B. K., Michel-Dansac, L., et al. 2012, MNRAS, 427, 1401

Cappellaro, E., Mazzali, P. A., Benetti, S., et al. 1997, A&A, 328, 203

Carraro, G., Lia, C., & Chiosi, C. 1998, MNRAS, 297, 1021

Chiappini, C., Matteucci, F., & Romano, D. 2001, ApJ, 554, 1044

Croom, S. M., Lawrence, J. S., Bland-Hawthorn, J., et al. 2012, MNRAS, 421, 872

De Lucia, G., Tornatore, L., Frenk, C. S., et al. 2014, MNRAS, 445, 970

Few, C. G., Courty, S., Gibson, B. K., Michel-Dansac, L., & Calura, F. 2014, MNRAS, 444, 3845

Fioc, M., & Rocca-Volmerange, B. 1997, A&A, 326, 950

François, P., Matteucci, F., Cayrel, R., et al. 2004, A&A, 421, 613

Gargiulo, I. D., Cora, S. A., Padilla, N. D., et al. 2015, MNRAS, 446, 3820

Geier, S., Marsh, T. R., Wang, B., et al. 2013, A&A, 554, A54

Greggio, L. 1996, in The Interplay Between Massive Star Formation, the ISM and Galaxy Evolution, ed. D. Kunth, B. Guiderdoni, M. Heydari-Malayeri, & T. X. Thuan, 89

Greggio, L. 2005, A&A, 441, 1055

—. 2010, MNRAS, 406, 22

Greggio, L., & Renzini, A. 1983, A&A, 118, 217

Hachisu, I., Kato, M., & Nomoto, K. 1996, ApJ, 470, L97

—. 1999, ApJ, 522, 487

Han, Z., & Podsiadlowski, P. 2004, MNRAS, 350, 1301

Hoyle, F., & Fowler, W. A. 1960, ApJ, 132, 565

Iben, Jr., I., & Tutukov, A. V. 1984, ApJS, 54, 335

Iwamoto, K., Brachwitz, F., Nomoto, K., et al. 1999, ApJS, 125, 439

Jiménez, N., Cora, S. A., Bassino, L. P., Tecce, T. E., & Smith Castelli, A. V. 2011, MNRAS, 417, 785

Kennicutt, Jr., R. C. 1998, ApJ, 498, 541

Kobayashi, C. 2004, MNRAS, 347, 740

Kobayashi, C., Tsujimoto, T., Nomoto, K., Hachisu, I., & Kato, M. 1998, ApJ, 503, L155

Kroupa, P. 2001, MNRAS, 322, 231

Lecureur, A., Hill, V., Zoccali, M., et al. 2007, A&A, 465, 799

Li, W., Chornock, R., Leaman, J., et al. 2011, MNRAS, 412, 1473

Longhetti, M., & Saracco, P. 2009, MNRAS, 394, 774

Lorén-Aguilar, P., Isern, J., & García-Berro, E. 2010, MNRAS, 406, 2749

Maiolino, R., Schneider, R., Oliva, E., et al. 2004, Nature, 431, 533

Mannucci, F., Della Valle, M., & Panagia, N. 2006, MNRAS, 370, 773

Mannucci, F., Della Valle, M., Panagia, N., et al. 2005, A&A, 433, 807

Maoz, D., Mannucci, F., & Brandt, T. D. 2012, MNRAS, 426, 3282

Maoz, D., Mannucci, F., & Nelemans, G. 2013, ArXiv e-prints, arXiv:1312.0628

Matteucci, F. 1994, A&A, 288, 57

Matteucci, F., & Brocato, E. 1990a, ApJ, 365, 539

—. 1990b, ApJ, 365, 539

Matteucci, F., & Greggio, L. 1986, A&A, 154, 279

Matteucci, F., Panagia, N., Pipino, A., et al. 2006, MNRAS, 372, 265

Matteucci, F., & Recchi, S. 2001, ApJ, 558, 351

Matteucci, F., Spitoni, E., Recchi, S., & Valiante, R. 2009, A&A, 501, 531

McWilliam, A., Matteucci, F., Ballero, S., et al. 2008, AJ, 136, 367

Mosconi, M. B., Tissera, P. B., Lambas, D. G., & Cora, S. A. 2001, MNRAS, 325, 34

Nagashima, M., Lacey, C. G., Baugh, C. M., Frenk, C. S., & Cole, S. 2005, MNRAS, 358, 1247

Nakasato, N., & Nomoto, K. 2003, ApJ, 588, 842

Navarro, J. F., Frenk, C. S., & White, S. D. M. 1997, ApJ, 490, 493

Padovani, P., & Matteucci, F. 1993, ApJ, 416, 26

Pan, T., Kasen, D., & Loeb, A. 2012, MNRAS, 422, 2701

Perez, J., Michel-Dansac, L., & Tissera, P. B. 2011, MNRAS, 417, 580

Perez, J., Valenzuela, O., Tissera, P. B., & Michel-Dansac, L. 2013, MNRAS, 436, 259

Perlmutter, S., Turner, M. S., & White, M. 1999, Physical Review Letters, 83, 670

Pietrinferni, A., Cassisi, S., Salaris, M., & Castelli, F. 2006, ApJ, 642, 797

Pipino, A., & Matteucci, F. 2004, MNRAS, 347, 968

Pritchet, C. J., Howell, D. A., & Sullivan, M. 2008, ApJ, 683, L25

Raiteri, C. M., Villata, M., & Navarro, J. F. 1996, A&A, 315, 105

Rest, A., Scolnic, D., Foley, R. J., et al. 2013, ArXiv e-prints, arXiv:1310.3828

Rojas-Arriagada, A., Recio-Blanco, A., Hill, V., et al. 2014, ArXiv e-prints, arXiv:1408.4558

Salpeter, E. E. 1955, ApJ, 121, 161

Sanchez, S. F., Rosales-Ortega, F. F., Iglesias-Paramo, J., et al. 2013, ArXiv e-prints, arXiv:1311.7052

Scannapieco, C., Tissera, P. B., White, S. D. M., & Springel, V. 2005, MNRAS, 364, 552

—. 2006, MNRAS, 371, 1125

—. 2008, MNRAS, 389, 1137

Scannapieco, C., White, S. D. M., Springel, V., & Tissera, P. B. 2009, MNRAS, 396, 696

Schmidt, M. 1959, ApJ, 129, 243

Shen, K. J., Guillochon, J., & Foley, R. J. 2013, ApJ, 770, L35

Smith, M., Nichol, R. C., Dilday, B., et al. 2012, ApJ, 755, 61

Soker, N., García-Berro, E., & Althaus, L. G. 2013, MNRAS, arXiv:1309.0368

Springel, V. 2005, MNRAS, 364, 1105

Sullivan, M., Le Borgne, D., Pritchet, C. J., Hodsman, A., & Neill. 2006, ApJ, 648, 868

Sutherland, R. S., & Dopita, M. A. 1993, ApJS, 88, 253

Tinsley, B. M. 1979, ApJ, 229, 1046

Tissera, P., Beers, T., Carollo, D., & Scannapieco, C. 2013a, ArXiv e-prints, arXiv:1309.3609

Tissera, P. B., Beers, T. C., Carollo, D., & Scannapieco, C. 2014, MNRAS, 439, 3128

Tissera, P. B., Scannapieco, C., Beers, T. C., & Carollo, D. 2013b, MNRAS, 432, 3391

Tissera, P. B., White, S. D. M., & Scannapieco, C. 2012, MNRAS, 420, 255

Tornambe, A., & Matteucci, F. 1987, ApJ, 318, L25

Tornatore, L., Borgani, S., Matteucci, F., Recchi, S., & Tozzi, P. 2004, MNRAS, 349, L19

Totani, T., Morokuma, T., Oda, T., Doi, M., & Yasuda, N. 2008, PASJ, 60, 1327

Tsebrenko, D., & Soker, N. 2013, MNRAS, 435, 320

Tutukov, A. V., & Yungelson, L. R. 1980, Soviet Astronomy Letters, 6, 271

Valiante, R., Matteucci, F., Recchi, S., & Calura, F. 2009, New A, 14, 638

van den Bergh, S. 1991, ApJ, 369, 1

van den Heuvel, E. P. J., Bhattacharya, D., Nomoto, K., & Rappaport, S. A. 1992, A&A, 262, 97

Whelan, J., & Iben, Jr., I. 1973, ApJ, 186, 1007

White, S. D. M., & Frenk, C. S. 1991, ApJ, 379, 52

Wiersma, R. P. C., Schaye, J., Theuns, T., Dalla Vecchia, C., & Tornatore, L. 2009, MNRAS, 399, 574

Woosley, S. E., & Weaver, T. A. 1995, ApJS, 101, 181

Yates, R. M., Henriques, B., Thomas, P. A., et al. 2013, MNRAS, 435, 3500

Zoccali, M., Gonzalez, O. A., Vasquez, S., et al. 2014, ArXiv e-prints, arXiv:1401.4878

This 2-column preprint was prepared with the AAS LaTeX macros v5.2.

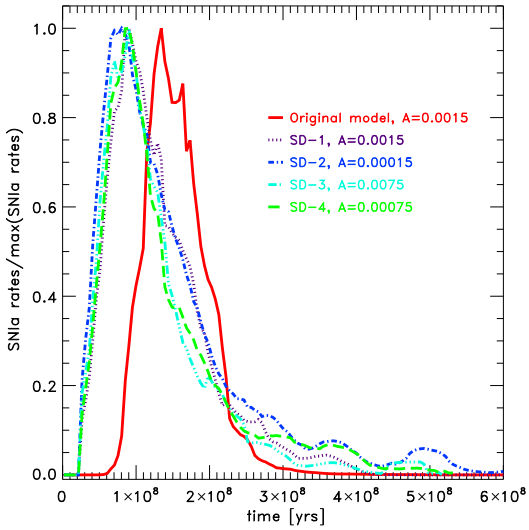


Fig. 2.— SNIa rates for all the models as function of time.

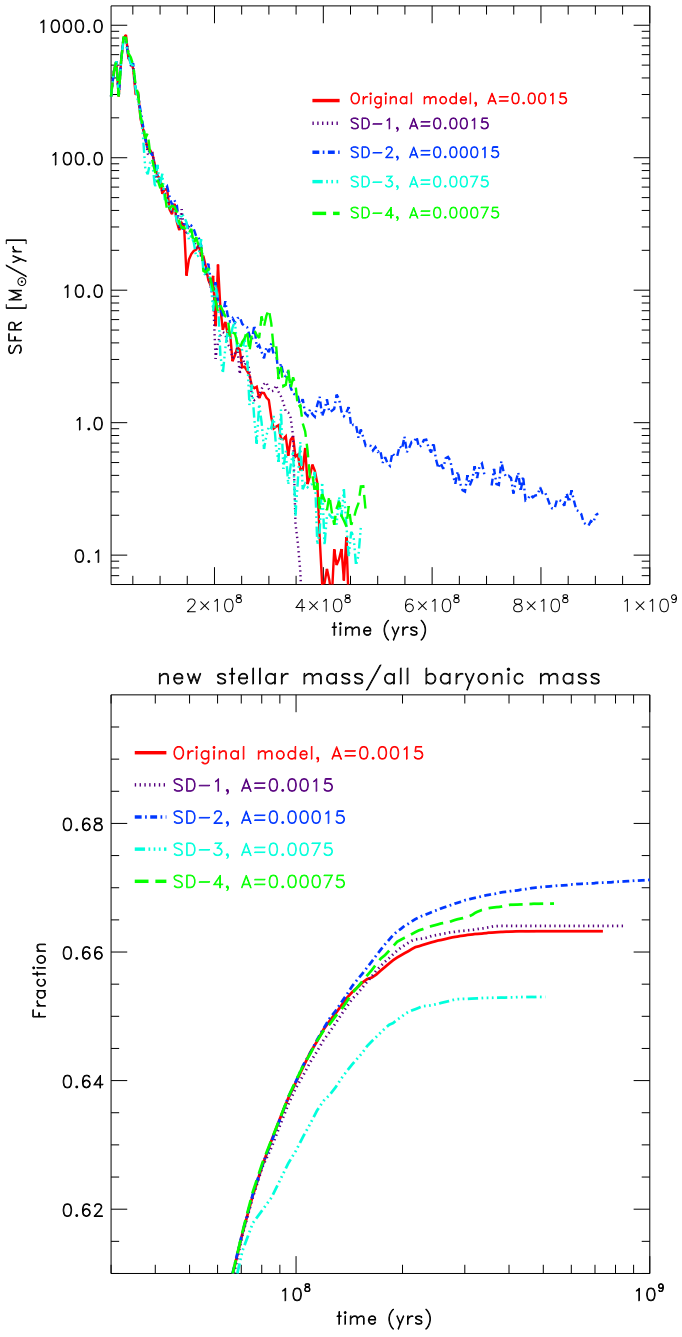


Fig. 3.— SFR history (upper panel) and mass fraction of new born stars (lower panel) for the SPH galaxies run with the same IC and varying the A values.

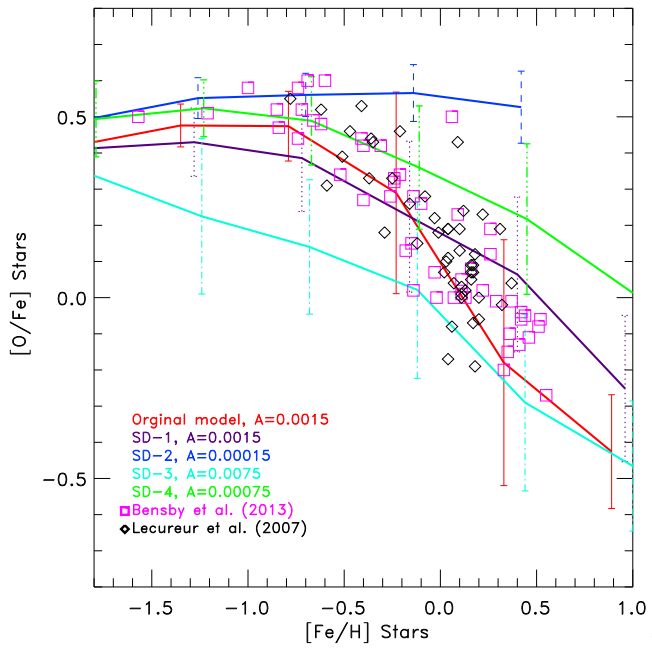


Fig. 4.— [O/Fe] vs. [Fe/H] exhibited by the bulge stars in the SPH simulated galaxies with the SD scenario by Matteucci & Recchi (2001) and varying A. These models are compared to observational [O/Fe] ratios for stars in the Galactic Bulge by Bensby et al. (2013); Lecureur et al. (2007). See Table 1 for details on the simulations.

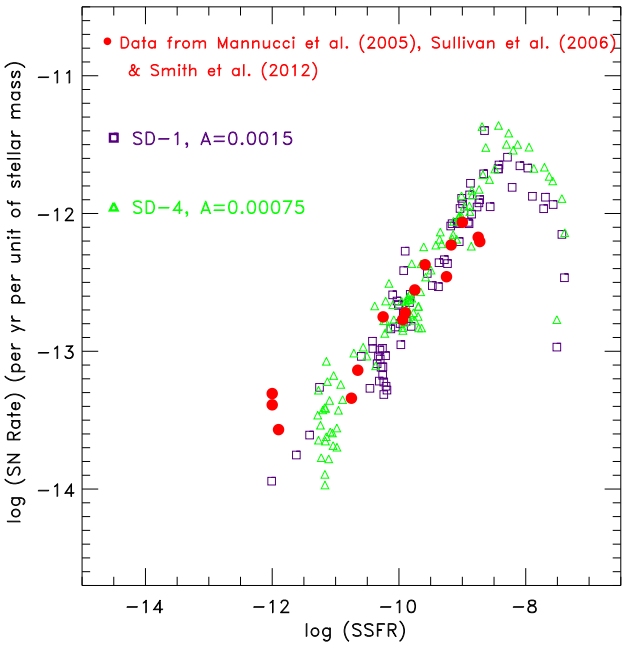


Fig. 5.— Specific star formation rate (SSFR) as a function of the SNIa rate per unit of galaxy mass (SSNIaR) for the SD-1 and SD-4 models (runs with A= 0.0015 and A= 0.00075). The red circles represent combined data from Sullivan et al. (2006); Mannucci et al. (2005); Smith et al. (2012). Notice that these models also fit the observed [O/Fe] ratios coming from the Galactic Bulge and the present-day SNIa rates. The zero-point has been renormalized by an *ad hoc* factor. See Section 5 for further details.

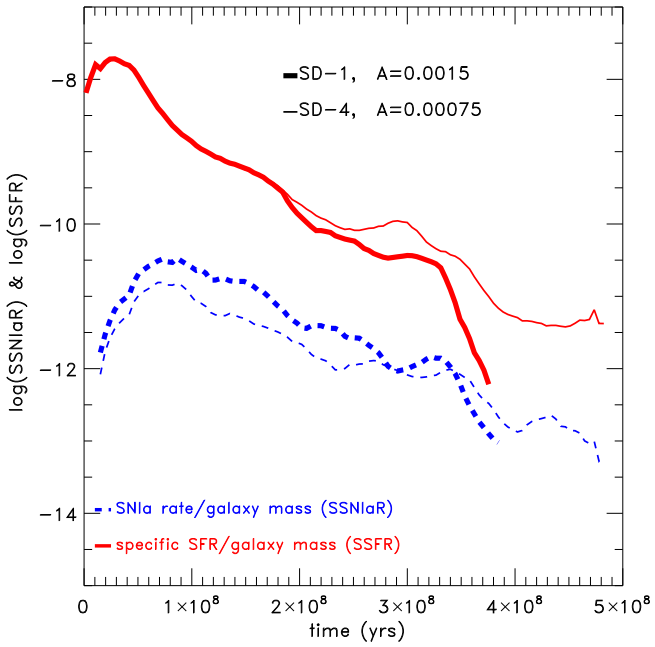


Fig. 6.— The log(SSFR)–continuous line–and log(SSNIaR) –dashed line–, evolving with time for our best models within the SD scenario (SD-1 and SD-4).